Bull Earthquake Eng (2010) 8:847–858
DOI 10.1007/s10518-009-9171-0

ORIGINAL RESEARCH PAPER

Simulating the Taipei basin response by numerical modeling of wave propagation

Joachim Miksat · Kuo-Liang Wen · Vladimir Sokolov · Chun-Te Chen · Friedemann Wenzel

Received: 5 February 2009 / Accepted: 14 December 2009 / Published online: 25 December 2009

Abstract Taipei, the capital of Taiwan, suffered from destructive earthquakes four times during the 20th century ($M_L = 7.3$ on April 15, 1909; $M_L = 6.8$ on November 15, 1986; the Chi–Chi $M_L = 7.3$ earthquake on September 21, 1999; and $M_L = 6.8$ on March 31, 2002). Analysis of recorded data shows a strong dependence of spectral amplification in the Taipei Basin on earthquake depth and azimuth. At low frequencies ($f < 3$ Hz) significant larger amplifications are observed for shallow earthquakes as compared to intermediate depth events. The former ones also display strong azimuthal dependence. As structures with large response periods such as bridges and tall buildings are sensitive to these low frequencies the understanding of the associated wave effects within the basin and their role for site effect amplification is critical. The tool we employ is 3D finite-difference modeling of wave propagation of incident wave fronts. The available detailed model of the basin allows studying the wave effects. Modeling clearly reveals that basin edge effects as observed in data are related to surface wave generation at the basin edges with a high degree of azimuthal dependency. The reproduced site amplification effects are in qualitative agreement with the observations from strong motion data.

Keywords Basin effects · Numerical modeling · Finite-differences · Wave propagation · Spectral amplifications

1 Introduction

During the 20th century four earthquakes caused severe damage in Taipei ($M_L = 7.3$ on April 15, 1909; $M_L = 6.8$ on November 15, 1986; the Chi–Chi $M_L = 7.3$ earthquake on September 21, 1999; and $M_L = 6.8$ on March 31, 2002). The city is located on a

J. Miksat (✉) · V. Sokolov · F. Wenzel
Karlsruhe Institute of Technology, Hertzstr. 16, 76187 Karlsruhe, Germany
e-mail: joachim.miksat@kit.edu

K.-L. Wen · C.-T. Chen
National Central University, Jhongli City, Taiwan (R.O.C)

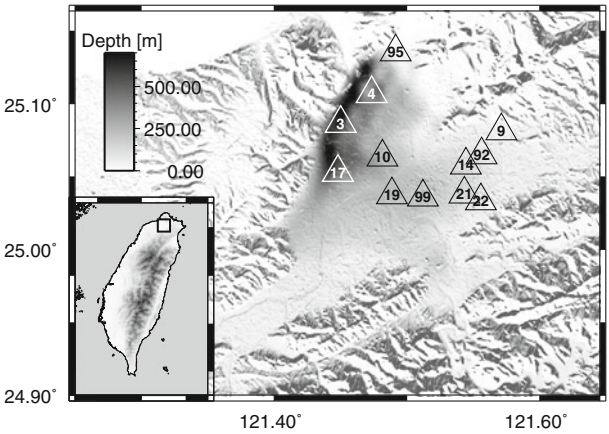

Fig. 1 Map of the triangle shaped Taipei basin in northern Taiwan. The depth to the Tertiary basement (Wang et al. 2004) is indicated by the *grayscale*. Maximum depth is about 760 m along the western steep dipping margin of the basin. Maximum depth of the shallow flat eastern part is about 200 m. *Triangles* depict the stations of the TAP network that are evaluated in this paper

sedimentary basin, which can be divided in a deep western, with steep dipping edges, and a shallow eastern part (Fig. 1). The basin structure is well known and based on reflection and borehole data (Wang et al. 2004). The whole Taipei region is covered with a dense strong motion network which is operated in the frame of the TSMIP (Taiwan Strong Motion Instrumentation Program) conducted by the CWB (Central Weather Bureau). Recent analysis of recorded data (Sokolov et al. 2008, 2009; Chen, manuscript in preparation, 2009) showed that shallow earthquakes cause large amplifications in the low frequency range. Furthermore, amplifications show a clear azimuthal dependence. In order to understand the observed ground motion characteristics, we perform 3D finite-difference (FD) simulations of an incident S-wave front on the basin for different azimuths and incidence angles corresponding to deep and shallow earthquakes. The simulations are performed for the 3D basin structure and a homogeneous model that reflects hard rock conditions. This enables us to examine the influence of the 3D basin structure. For the Taipei basin several modeling studies on wave propagation simulations have been performed recently (Lee et al. 2008a,b, 2009). These studies focus mainly on the description of wave propagation and the influence of different subsurface structures on the resulting ground motions by exploring wave forms, peak ground accelerations (PGA), peak ground velocities (PGV), snapshots of the wave field and cumulative energy. In this publications we address the question whether numerical modeling of wave propagation can explain the peculiarities of spectral amplification found by the analysis of empirical data. We also examine whether numerical modeling of wave propagation can be successfully applied to calculate site amplification for the Taipei basin. Compared to 1D analysis of site effects such numerical simulations include also 3D effects due to the basin structure as well as basin induced surface waves which allows a more reliable site amplification estimation for complicated subsurface structures.

2 Observations

Analysis of empirical data have been performed by applying the VHR method (Sokolov et al. 2000). Sokolov et al. (2008, 2009) found that spectral ratios for stations in the central part of the basin are larger for shallow than for deep earthquakes for frequencies up to 3 Hz. For stations located directly along the basin edges, no clear difference is observable. Chen (manuscript in preparation, 2009) explored the depth and azimuthal dependence of H/V ratios for stations in the Taipei basin. In general, large H/V values are obtained at stations near the basin center for shallow earthquakes. Like the VHR ratios, H/V results do not show significant

difference between deep and shallow earthquakes at the basin edges. Additionally, a clear azimuthal dependence of the VHR and H/V ratios was observed.

3 Taipei basin model

The knowledge of the underground structure is essential for FD simulations of wave propagation. The detailed structure of the Taipei basin is known from shallow reflection seismic experiments and from borehole drilling data (Wang et al. 2004). The triangle shaped basin is floored by a Tertiary basement with maximum depth of about 700 m in the northwest. The basin was formed by subsidence along the Sanchiao fault, now marked by the northwest border of the basin (Teng et al. 2001). Then the basin was filled by alluvium deposits which resulted in flat-lying Quaternary layers. Based on the given depths of the Tertiary basement (see Fig. 1) and the SRTM (Shuttle Radar Topography Mission) 90 m (CIAT 2004) data, we constructed the sediment-bedrock boundary layer. From the data given in Wang et al. (2004), we calculated a velocity-depth function in order to assign proper P- and S-wave velocities for the basin. Minimum shear wave velocity of the model is 170 m/s, which corresponds to the average surface velocity of the the uppermost layer, the so called Sungshan formation, derived by Wang et al. (2004). Figure 2 displays the created basin structure and shear wave velocities for the NW profile. For the FD simulations the model is discretized with 50 and 25 m in horizontal and vertical direction, respectively. The horizontal (EW and NS) extensions of the model are 29.8–29.8 km. Model depth depends on incidence angle of the S-wave front and varies between 2.6 and 16.4 km. Our Taipei basin model is based on the same input data (Wang et al. 2004) as the model used by Lee et al. (2008a). However, Lee et al. (2008a) used minimum shear wave velocities of 260 and 866 m/s compared to 170 m/s in our study.

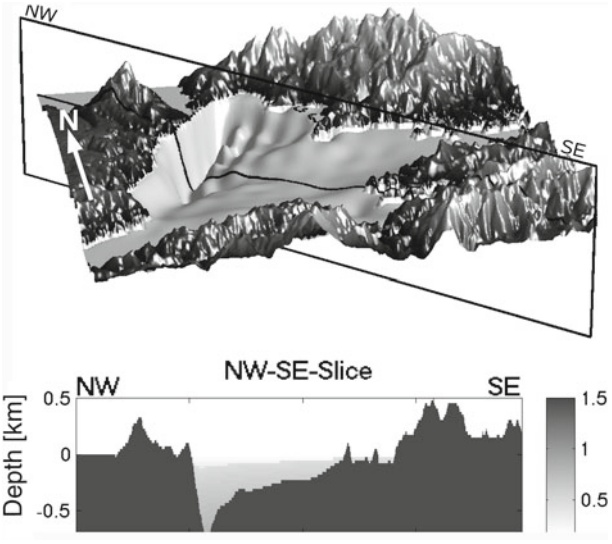

Fig. 2 *Top*: created basin-topography structure from SRTM topography data CIAT (2004) and the basement structure given by Wang et al. (2004). *Bottom*: shear wave velocities along the NW profile. Shear wave velocity ranges from 0.17 km/s (*uppermost sediments*) to 1.5 km/s (*basement*)

Table 1 Modeling parameters

Horizontal discretization (m)	50
Vertical discretization (m)	25
Number of grid points (EW-direction)	596
Number of grid points (NS-direction)	596
Number of grid points (z-direction)	104–656
Horizontal extension in EW-direction (km)	29.8
Horizontal extension in NS-direction (km)	29.8
Vertical extension in z-direction (km)	2.6–16.4
Minimum shear wave velocity (m/s)	170
Temporal discretization (ms)	3
Number of time steps	15,000–20,000
Simulation time (s)	45–60

Furthermore, the final models may also differ because of different boundary conditions for the interpolation procedures.

4 Numerical modeling

We use a 3D FD method (Furumura and Chen 2005; Furumura and Kennett 2005) in order to simulate wave propagation for the Taipei basin. The code is 4th (vertical direction) to 16th (horizontal direction) order in space and second order in time. Three grid points per minimum wavelength in horizontal and six grid points per minimum wavelength in vertical direction are required in order to obtain reliable results (Furumura and Chen 2004). A list of modeling parameters is given in Table 1. Based on the minimum shear wave velocity and grid spacing, maximum frequency of our simulations is 1 Hz. At the sides and the bottom of the model damping (Cerjan et al. 1985) and one-way absorbing (Clayton and Enquist 1977) boundary conditions are applied. Recently we simulated a real seismic event that occurred close to the Taipei basin on October 23, 2004 to validate the model as well as the applied numerical 3D FD method (Miksat et al. 2009, in preparation). This analysis showed a good fit between observed and simulated waveforms which supports the reliability and accuracy of the applied modeling method.

The aim of our study is a qualitative comparison of site amplifications obtained from empirical data and numerical modeling. The analysis of empirical data included records from about 220 earthquakes. Numerical simulation for all of these earthquakes would exceed the available computer resources. Furthermore, the limited knowledge of the regional structure outside the basin, especially of the Q-structure, and source parameters (fault plane solution and stress drop) wouldn't allow an accurate modeling of absolute ground motions. Uncertainties of these parameters may be projected into the basin and misinterpreted as basin effects. Therefore, we decided to simulate planar S-wave front incidence on the basin and explore only the basins influence on incoming S-waves. By comparing the simulations with reference simulations for homogeneous subsurface structures we can calculate relative effects. The seismic wave velocities of the homogeneous model ($v_p = 3$ km/s, $v_s = 1.5$ km/s) correspond to the bedrock velocities in the Taipei basin model. In our study we distinguish deep and shallow earthquakes. Deep earthquakes are simulated by wave front incidence from the bottom (incidence angle $i = 0°$ measured between wave front and surface) and

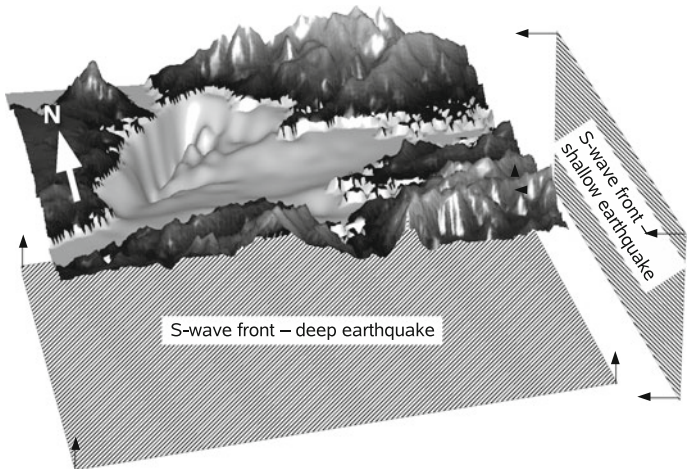

Fig. 3 We simulate distant deep earthquakes by planar S-wave front incidence from the bottom and shallow earthquakes by S-wave front incidence from the East and South

Table 2 Scenarios

Scenario earthquake	$M_{ij} = 1$	Source component	Incidence angle
Deep/distant	M_{xz}, M_{zx}	x (EW)	0°
Shallow south	M_{xz}, M_{zx}	x (EW)	90°
Shallow east	M_{yz}, M_{zy}	y (NS)	90°

shallow earthquakes correspond to an incidence angle of 90° (see Fig. 3). Seismicity mainly occurs east and south of the Taipei basin. Therefore, we also explore the azimuthal dependence of the basin response by simulating wave front incidence for shallow earthquakes for azimuths of 90° and 180°. Details for all scenarios are given in Table 2. For each source grid point of the implemented planar wave front, a double couple source is applied so that a pure S-wave front results in propagation direction. The resulting S-wave polarization of the source depends on the actual choice of the applied moment tensor components. In this paper we simulate wave propagation for SH-polarized wave fronts. The source time function of the added stress glut (see Miksat et al. 2008; Olsen et al. 2006) at each grid point of the source plane is described by a Herrman window with a width of 0.5 s. The source time function and its Fourier amplitude spectra are shown in Fig. 4. Within the frequency range of interest the amplitude is almost constant except for frequencies larger than about 0.7 Hz. Frequency dependent spectral ratios are calculated by dividing the Fourier amplitude spectra (FAS) of the simulation for the 3D basin structure by the FAS resulting from the simulation for the homogeneous model. As both calculation include the same source time function the decline of the amplitude spectra for frequencies larger than 0.7 Hz does not influence the result because it is removed by the division operation. The obtained spectral amplifications reflect relative effects (amplification/deamplification) of the basin structure on incoming waves. These effects could be superimposed on existing standard hard rock attenuation relations in order to calculate absolute ground motion values within the basin.

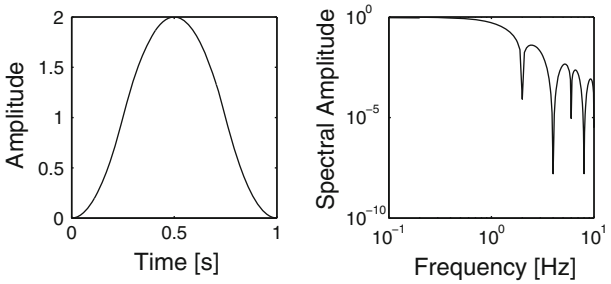

Fig. 4 Applied source time function and its Fourier amplitude spectrum

5 Results

5.1 Spectral amplifications

Figure 5 shows modeled spectral ratios at several stations (station locations are depicted in Fig. 1). The stations are located in the deepest part of the basin, in the eastern shallow part and near the basin edges. In general, we obtain larger spectral ratios for the shallow earthquakes than for the deep earthquake at stations within the basin. However, for stations near the basin edges the spectral amplifications are similar for the deep and shallow scenarios east of the basin. The shallow scenario south of the basin produces only small ground shaking at TAP 95 and TAP 9, which are located at points along the northern margin of the basin. Therefore, only small spectral amplifications are obtained at this stations for wave incidence from the South. Looking at the dominant frequency, maximum ratios change from 0.3 Hz for stations located in the western deep part of the basin to 0.3–0.6 Hz for the central and eastern part. Along the basin edges the maximum is obtained for frequencies larger than 0.6 Hz. This frequency dependence was also found by Sokolov et al. (2008, 2009) from analysis of empirical data. The spectral ratios also reveal azimuthal effects at stations TAP 17 and TAP 92. For TAP 17, which is located in the southwest of the basin, earthquakes south of the basin produce stronger amplifications than earthquakes east of the basin. This is interchanged at station TAP 92 in the eastern part of the basin, where earthquakes east of the basin produce strongest amplifications.

5.2 Wave field

Next we look at snapshots of the wave field for all three scenarios (Fig. 6). We show for each scenario the component of the wave field that is equal to the polarization of the implemented S-wave front. This is EW for the deep and shallow scenario south of the basin and NS for the scenario east of the basin (see Table 2). The velocities are scaled to the maximum velocity at the marked hard rock (HR) station outside the basin (black triangle). The snapshots show clearly the generation of surface waves at the southern and eastern basin edges for both shallow scenarios. For the earthquakes in the South, strongest surface waves amplitudes are generated in the south-western edge of the basin and guided along the deep part of the basin to the North (solid marked). When the earthquake occurs east of the basin, strong surface waves are excited at the eastern edge and at the eastern rim of the northern embayment of the basin and travel to the western deepest part of the basin (solid marked areas). The waves generated at the easternmost edge of the basin are guided to the West along a deep channel through the

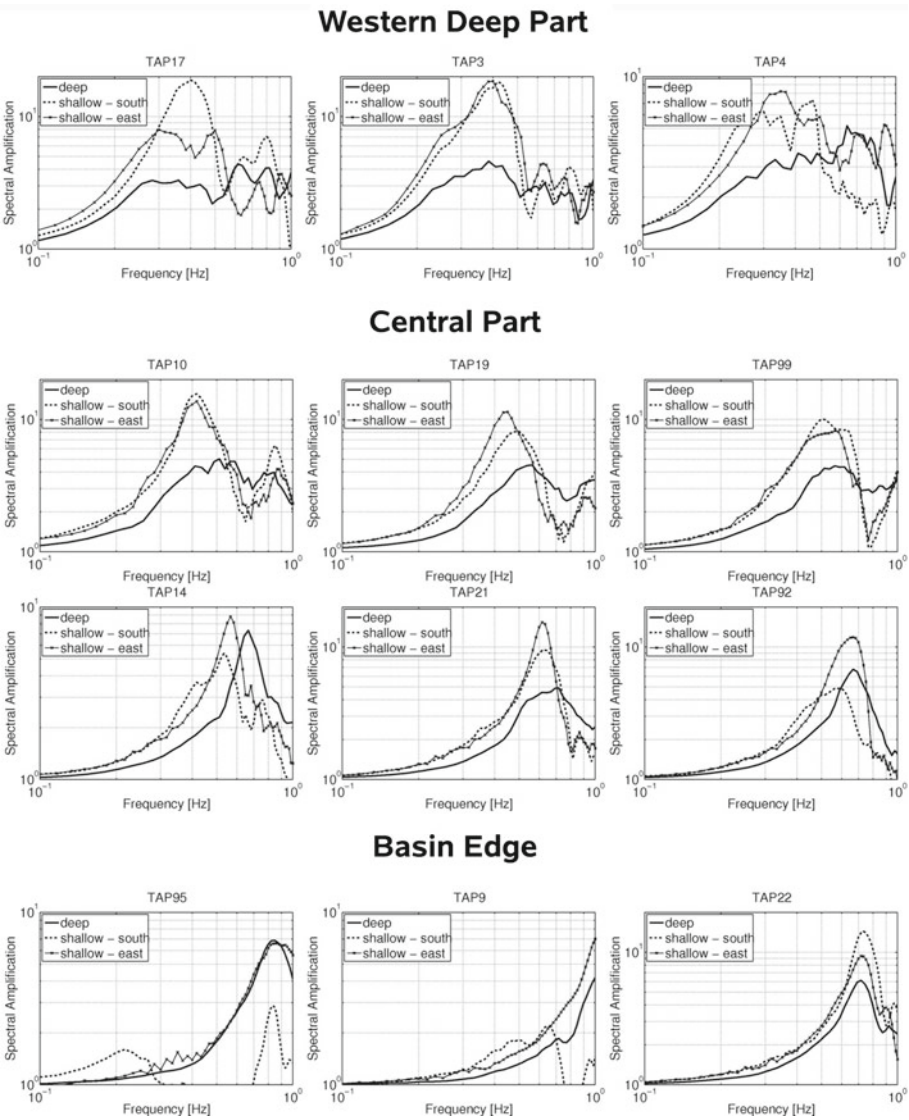

Fig. 5 Modeled spectral amplification for the shallow and deep scenario. The station locations are given in Fig. 1. For stations in the western and central part, the amplifications of the shallow scenario are clearly larger than for the deep event. Maximum amplification occurs for stations at the deepest part at 0.3–0.4 Hz and for stations in the central part for 0.4–0.6 Hz. For stations at the basin edge, spectral amplifications are similar for the deep and shallow scenario

center of the basin. Compared to the deep scenario both shallow scenarios produce stronger surface waves and significant longer ground motion. Therefore, the larger spectral amplifications for shallow earthquakes can be explained by the generation of surface waves at the basin margins. The azimuthal dependence of surface wave generation and main travel paths through the basin explain the above discussed azimuth dependent spectral amplifications at some stations. For TAP 17, which is located in the southwest of the basin, earthquakes south

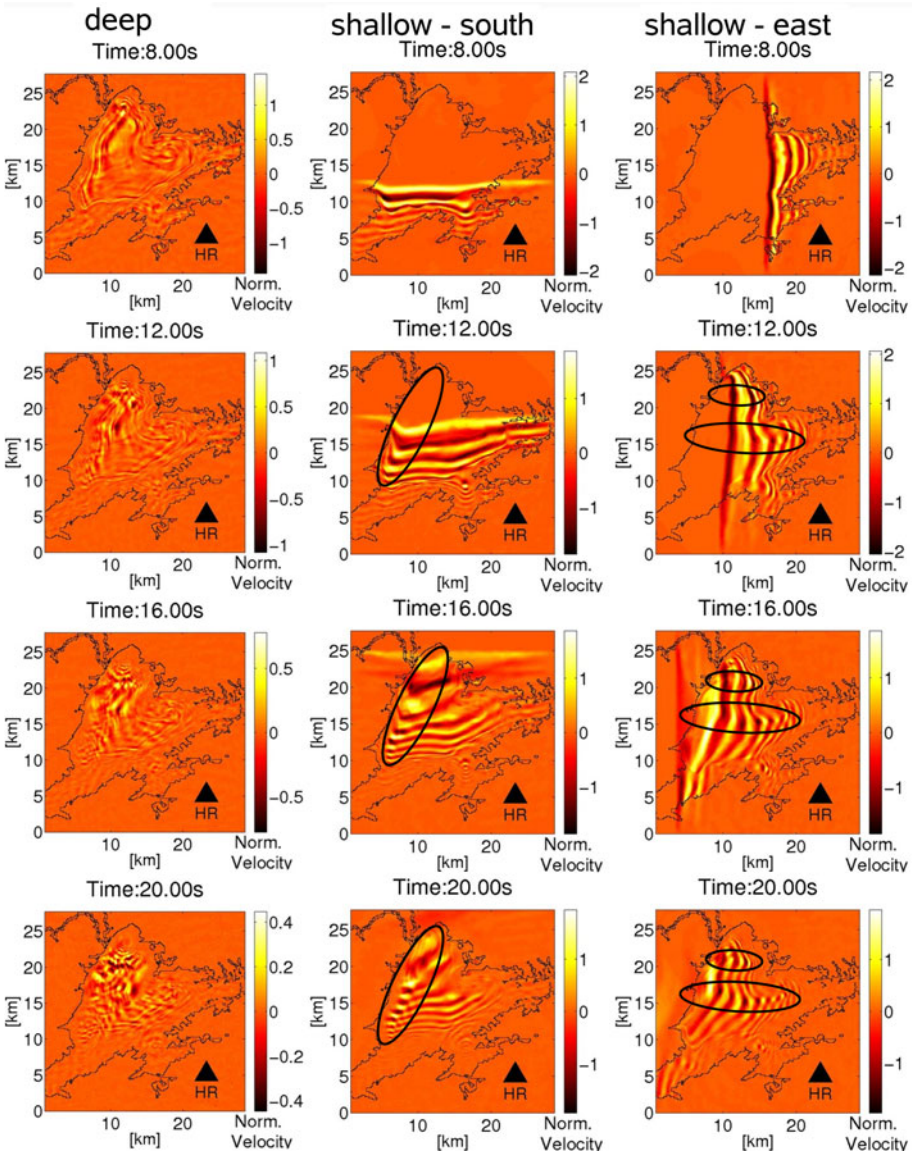

Fig. 6 Snapshots of the wave field after 8, 12, 16 and 20 s with wave incidence for deep (*left*) and shallow earthquakes in the South (*center*) and East (*right*). Strong surface waves are generated at the southern and eastern basin edges for the scenario in the South and East, respectively. Along their travel paths (*solid marked*) they produce strong and long ground shaking. Velocity is scaled to the PGV at the indicated hard rock (*H R*) station outside the basin

of the basin produce large amplitudes and long ground shaking. On the other hand, station TAP 92 in the eastern part of the basin shows larger spectral amplifications for earthquakes east of the basin because of surface waves generated along the eastern basin margin. Stations that are more in the central part of the basin show almost no azimuthal dependence. Significant durations (Chen and Scawthorn 2003) are calculated for both shallow scenarios (Fig. 7).

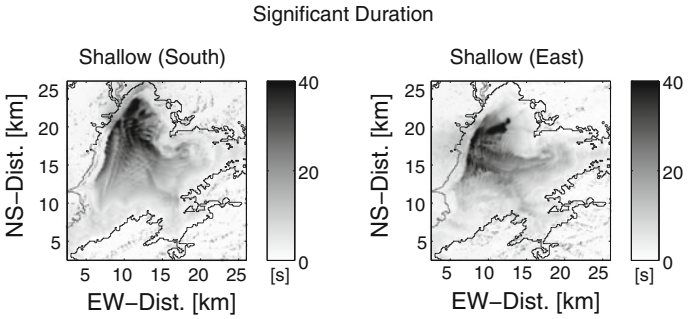

Fig. 7 We calculate significant duration after Chen and Scawthorn (2003) for the shallow scenarios south (*left*) and east (*right*) of the basin. Especially, for the shallow scenario east of the basin the main travel paths of the strong surface waves are clearly visible (compare with Fig. 6). Furthermore, significant duration shows also strong earthquake azimuth dependence. Whereas durations in the western central part are similar for both cases, significant duration is clearly longer in the northern part of the basin for wave incidence from the South

Maximum duration is about 40 s in both cases. The durations show also a strong earthquake azimuth dependence. This is especially the case for the northern part of the basin, where significant duration is about 40 s for the scenario south of the basin and about 10 s for wave incidence from the East. The main travel paths found in Fig. 6 of the strong surface waves are also clearly visible for the scenario east of the basin. Unfortunately, we cannot compare our simulation results with real data as there is no study on ground shaking duration available.

We can see similarities between our snapshots of the wave front from the East and South and the results given by (Lee et al. 2008b, Fig. 4). In both studies the primary S-waves are followed by surface waves. Surface wave travel along preferred path through the basin and strongest ground shaking is obtained for the western deep part of the basin. We can compare significant duration (Fig. 7) and cumulative energy in (Lee et al. 2008b Fig. 6), which are related quantities. From both studies it is obvious that maximum values are located in all cases (wave front from the East and South in this study; scenario earthquake south-east of the basin in Lee's work) in the western deep part of the basin. On the other hand the above described preferred travel paths from the basin edge to the western deep part, which are also visible when looking at significant duration and cumulative energy, depend strongly on earthquake azimuth.

5.3 Comparison with observed spectral ratio

In Fig. 8, we compare observed and modeled spectral amplification at 0.5 Hz. The modeling results of all three scenarios have been averaged. The observed ratios are based on earthquake records of the TSMIP network (Wen et al. 2007; Wen and Peng 1998). Our modeling shows a good comparison with the observations. In both cases maximum values are obtained along the western deep part of the basin and in the eastern shallow part of the basin. In general, absolute values are in good agreement with the observed ratios. Our modeling underestimates the observed values in the northern part and the modeled maximum values in the eastern part are shifted to the West compared to the observed ratios. This can be explained by the used constant surface velocity of 170 m/s, which is an average value of the Sungshan layer, in contrast to the real varying surface velocities with values of about 100 m/s in the eastern part of the basin. Also the usage of only two different earthquake azimuths to reflect the real seismicity distribution can produce the observed discrepancy. Future studies should focus

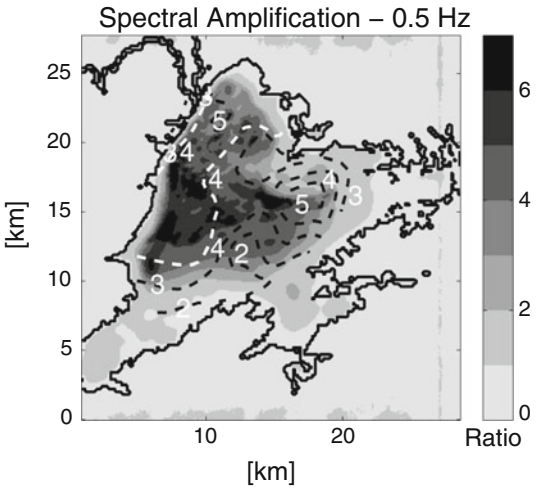

Fig. 8 Modeled (*gray scale*) and observed spectral amplifications (*contour lines*). The modeling reproduces the observed absolute values and shows, as the observation, main areas of large amplifications in the western deep part of the basin and in the eastern shallow part of the basin. However, the region of modeled maximum amplifications in the eastern part of the basin is shifted to the west relatively to the observations. This is most likely due to the difference between the applied average surface velocities (170 m/s) for the whole basin and the real low surface velocities (≈100 m/s) in the eastern part of the basin

on a more detailed analysis of earthquake azimuth dependence of spectral amplifications by simulating wave incidence for many different azimuths in order to resolve this issue.

6 Discussion and conclusion

We calculate the Taipei basin response by simulating planar S-wave front incidence in order to identify first-order effects in a qualitative way. These first-order effects are the distinction between shallow and deep sources and the wave pattern they generate, particularly the surface wave effects once shallow earthquakes are involved. Another challenge is the more quantitative utilization of 3D modeling which is subject of future work.

We calculate site response in terms of relative effects (amplification factors) on an incoming S-wave by simulating planar S-wave front incidence on the basin and comparison with simulations for a homogeneous subsurface structure. In order to obtain absolute ground motion values within the basin the calculated relative effects could be superimposed on existing standard hard rock attenuation relations. Our approach excludes path and source effects, which may have influence on the resulting ground motion within the basin. As the subsurface structure, especially the Q structure, outside the Taipei basin and the source parameter (fault orientation, stress drop) are not well known the simulations of specific distant earthquakes may project uncertainties due to this limited knowledge into the basin on the calculated ground motions. Therefore, we decided to apply the planar wave front incidence approach for the 3D structure and a homogeneous structure and to calculate relative basin effects rather than absolute ground motions.

The modeling explains the observations based on VHR and H/V ratios qualitatively. As reliable spectral amplifications from observations are only available for 0.5 Hz in the simulated low frequency range, a more quantitative comparison between observation and modeling could only be performed for this frequency. Consequently, the calculation of spectral amplifications by using more high performance computing capacities for a broader frequency range up to several Hz should be of high priority for future simulations. This would allow a more thorough analysis of the reliability of the modeling results. For 0.5 Hz the spatial distribution

of spectral amplifications as well as the absolute amplification ratios are reproduced by the modeling.

Our simulations show that for the Taipei basin, generation of large amplitude surface waves occur for shallow earthquakes. Furthermore, areas that suffer from strong and long shaking duration depend on earthquake azimuth. Consequently, the influence of earthquake azimuth has to be implemented in any hazard assessment for the Taipei basin in order to obtain reliable results. The Taipei basin example shows that for a detailed knowledge of the basin structure, site response can be derived by 3D numerical simulation of wave propagation for an incident S-wave front. Therefore, this approach could be a very valuable tool for regions where the basin structure is known from geophysical campaigns but the database of observations is very sparse because of short observation times or low seismicity.

Acknowledgments We thank T. Furumura for providing his 3D finite-difference code. We also thank C. Y. Wang for providing the Taipei basin model. The simulations have been carried out on the HP XC6000 system of the Scientific Supercomputing Center Karlsruhe, Germany. This work was funded by the Deutsche Forschungsgemeinschaft, Germany (DFG - project WE 1394/13-1) and the National Science Council, Taiwan, ROC (grant NSC 96-2119-M-008-007). We thank an anonymous reviewer for his very valuable comments that allowed to improve the manuscript significantly.

References

Cerjan C, Kosloff D, Kosloff R, Reshef M (1985) A nonreflecting boundary condition for discrete and elastic wave equations. Geophysics 50(4):705–708

Chen WF, Scawthorn C (eds) (2003) Earthquake engineering handbook. CRC Press LLC, Boca Raton

CIAT (2004) Void-filled seamless SRTM data v1, 2004, International centre for tropical agriculture (CIAT). Available from the CGIAR-CSI SRTM 90m Database: http://srtm.csi.cgiar.org

Clayton R, Enquist B (1977) Absorbing boundary conditions for acoustic and elastic wave equations. Bull Seism Soc Am 67(6):1529–1540

Furumura T, Chen L (2004) Large scale parallel simulation and visualization of 3-D seismic wavefield using the Earth Simulator. Comput Model Eng Sci 6(2):153–168

Furumura T, Chen L (2005) Parallel simulation of strong ground motions during recent and historical damaging earthquakes in Tokyo, Japan. Parallel Comput 31(2):149–165

Furumura T, Kennett K (2005) Subduction zone guided waves and the heterogeneity structure of the subducted plate: Intensity anomalies in northern Japan. J Geophys Res 110:B10,302

Lee SJ, Chen HW, Huang BS (2008) Simulations of strong ground motion and 3D amplification effect in the Taipei basin by using a composite grid finite-difference method. Bull Seism Soc Am 98(3):1229–1242. doi:10.1785/0120060098

Lee SJ, Chen HW, Liu Q, Komatitsch D, Huang BS, Tromp J (2008) Three-dimensional simulations of seismic-wave propagation in the Taipei basin with realistic topography based upon the spectral-element method. Bull Seism Soc Am 98(1):253–264. doi:10.1785/0120070033

Lee SJ, Chan YC, Komatitsch D, Huang BS, Tromp J (2009) Effects of realistic surface topography on seismic ground motion in the Yangminshan region of Taiwan based upon the spectral-element method and LiDAR DTM. Bull Seism Soc Am 99(2A):681–693. doi:10.1785/0120080264

Miksat J, Müller T, Wenzel F (2008) Simulating 3D seismograms in 2.5D structures by combining 2D finite-difference modeling and ray tracing. Geophys J Int 174(1):309–315. doi:10.1111/j.1365-246X.2008.03800.x

Olsen KB, Akinci A, Rovelli A, Marra F, Malagnini L (2006) 3D ground-motion estimation in Rome, Italy. Bull Seism Soc Am 96(1):133–146. doi:10.1785/0120030243

Sokolov V, Wen KL, Miksat J, Wenzel F, Chen CT (2008) Analysis of Taipei basin response on earthquakes of various depth and location using empirical data. paper presented at 31st General Assembly of the European Seismological Commission ESC 2008, Hersonissos, Greece, 7–12 September, pp 435–442

Sokolov V, Wen KL, Miksat J, Wenzel F, Chen CT (2009) Analysis of Taipei basin response on earthquakes of various depth and location using empirical data. Terr Atmos Ocean Sci 20(5): 687–702. doi:10.3319/TAO.2008.10.15.01(T)

Sokolov VY, Loh CH, Wen KL (2000) Empirical study of sediment-filled basin response: the case of Taipei city. Earthquake Spectra 16(3):681–707. doi:10.1193/1.1586134

Teng LS, Lee CT, Peng CH, Chen WF, Chu CJ (2001) Origin and geological evolution of the Taipei basin, northern Taiwan. West Pac Earth Sci 1(2):115–142

Wang CY, Lee YH, Ger ML, Chen YL (2004) Investigating subsurface structures and P- and S-wave velocities in the Taipei Basin. Terr Atmos Ocean Sci 15(4):609–627

Wen KL, Peng HY (1998) Site effect analysis in the Taipei basin: results from TSMIP network data. Terr Atmos Ocean Sci 9(4):691–704

Wen KL, Lin CM, Chen CT (2007) Site response in the Taipei urban area from dense microtremor survey. paper presented at Fourth International Conference on Urban Earthquake Engineering, Center for Urban Earthquake Engineering, Tokyo Institute of Technology, Tokyo, Japan, 5–6 March, pp 139–146